Parameters influencing calcium phosphate precipitation in granular sludge sequencing batch reactor

Angela Mañas [a,b,c,d], Mathieu Pocquet [a,b,c], Béatrice Biscans [d,*], Mathieu Sperandio [a,b,c]

[a] Université de Toulouse, INSA, UPS, INP, LISBP, 135 Avenue de Rangueil, F-31077 Toulouse, France
[b] INRA, UMR 792 Ingénierie des Systèmes Biologiques et des Procédés, F-31400 Toulouse, France
[c] CNRS, UMR 5504, F-31400 Toulouse, France
[d] CNRS, Laboratoire de Génie Chimique, INP, UMR 5503, 4 allée Emile Monso BP 84234, F-31432 Toulouse Cedex 4, France

A B S T R A C T

Calcium phosphate precipitation inside microbial granules cultivated in a granular sequenced batch reactor (GSBR) has been demonstrated to contribute to phosphorus removal during wastewater treatment. Whereas hydroxyapatite (HAP) is proven to accumulate in the granule, the main calcium phosphate precursors that form prior to HAP are here investigated. A separate batch reactor was used to distinguish reactions involving biological phosphate removal from physicochemical reactions involving phosphate precipitation in order to establish the kinetics and stoichiometry of calcium phosphate formation. Experiments and simulations with PHREEQC and AQUASIM software support the assumption that amorphous calcium phosphate (ACP) is the intermediary in HAP crystallization. The results provide the kinetic rate constants and thermodynamic constants of ACP. The formation of bioliths inside biological aggregates as well as the main parameters that drive their formations are discussed here. Finally, the influence of pH and calcium and phosphate concentrations in the influent was also assessed, in order to determine the contribution of precipitation in the different operating conditions.

1. Introduction

A recent report of the *United Nations Environment Program* highlights phosphorus management as one of the main emerging problems to be faced in 2011 (United Nations of Environment Program Yearbook, 2011): the demand for phosphorus is increasing, the available resources are scarce, the use needs to become more efficient and the recycling more widespread. On the other hand, it is found in excess in wastewater effluents, damaging aquatic ecosystems and the quality of water. In a wastewater treatment plant, biological processes are mandatory for meeting carbon (COD) and nitrogen (N) quality standards of the effluent (Giesen, 1999). Biological dephosphatation by polyphosphate accumulating organisms (PAOs) have to be intensively employed but still needs to be combined with physicochemical treatment to isolate phosphate in a solid form. Therefore, research is now focusing increasingly on combined processes that remove phosphorous from wastewaters and successively recover it in the form of a valuable product (De-Bashan and Bashan, 2004), for example struvite ($MgNH_4PO_4 \cdot 6H_2O$) or hydroxyapatite ($Ca_5(PO_4)_3(OH)$).

The aerobic granular sludge process is a promising technology for wastewater treatment, performing simultaneous nitrogen and phosphorus removal (Liu and Tay, 2004; Lemaire, 2007; Morgenroth et al., 1997). The granular sludge process is based on dense microbial aggregates containing different bacterial communities. Recent studies indicate that calcium phosphate can also precipitate and accumulate in the core of granules, playing a role in the global performance of the process (Wan and Spérandio, 2009; Mañas et al., 2011). In this work, research focuses on this induced biological phosphorus precipitation inside biological aggregates. Until now, only a few studies have been dedicated to this mechanism (Dupraz et al., 2009; Bazylinski, 1996; Benzerara et al., 2011; Weiner, 2008), focusing on the general mineral precipitation on the walls of pure bacterial strains by changing either pH or ion concentration. This work aims to gain insight into the parameters that influence microbial induced phosphorus precipitation in granular sludge for wastewater treatment. Major questions concern the nature of the precursors in the Ca–P precipitation and the influence of the microbial reactions on the precipitation in relation with pH.

Previous work has identified the chemical composition of the mineral clusters found inside aerobic granules (Mañas et al., 2011). Hydroxyapatite (HAP) was the major crystallized compound and the presence of amorphous precipitates was also suggested by X-ray Diffraction Analysis. Boskey and Posner

* Corresponding author. Tel.: +33 5 34 32 36 38; fax: +33 5 34 32 37 00.
E-mail addresses: beatrice.biscans@ensiacet.fr, amanas_l@insa-toulouse.fr (B. Biscans).

(1974) and Nancollas and Koutsoukos (1980) stated that HAP could form without any precursors at low ionic strength (I_c) but its formation is normally preceded by different mineral phases depending on the pH, the ionic strength and the presence of other ions (Nancollas and Wu, 2000). Octacalcium phosphate (OCP) was identified as the precursor of HAP at physiological pH (Tomazic et al., 1975; Brown et al., 1981; Elliott, 1994). However, brushite (DCPD) was later reported by several authors (Abbona et al.,1986; Gao et al., 2010) as the hydroxyapatite precursor in acidic conditions, and OCP was also found to form in low-pH medium. Grases et al. (1996) found TCP to be a precursor of human calculi at pH between 6 and 7, although Johnsson and Nancollas (1992) stated that β-TCP is not formed at ambient temperature. Posner and Betts (1975) stated that HAP is preceded by a non or poor crystalline solid which consists of clusters with the formula: $Ca_9(PO_4)_6$. Finally, with a similar stoichiometry, amorphous calcium phosphate (ACP, $Ca_3(PO_4)_2 \cdot xH_2O$) was the most frequently reported precursor for HAP. It was first observed by Eanes et al. (1965) and, since then, several authors have observed it in different pH ranges: between pH=5 and 7.5, according to Lundager-Madsen et al. (1995) and Tsuge et al. (2002); in the neutral pH range (Lundager-Madsen and Christensson, 1991); at pH > 7.4, where ACP was the only phase reported by Monstastruc (2003) and Seckler et al. (1996) and even at high pH (9.5–12) in a report by Lazic (1995).

Normally, models consider the precipitation of the most thermodynamically stable phase as a function of the precursor formation but there is some disagreement about its choice. Maurer and Boller (1999) and Maurer et al. (1999) stated that calcium phosphate precipitation took place simultaneously with bio-dephosphatation processes throughout hydroxy dicalcium phosphate (HDP) formation but gave no demonstration to support their claim. In contrast Musvoto et al. (2000b) and Barat et al. (2011) assumed that ACP was the first calcium phosphate precursor. Musvoto et al. (2000b) succeeded in modeling phosphate precipitation in digester supernatant. Barat et al. (2011) showed that satisfying prediction of phosphorus removal by simultaneous biological and chemical processes was obtained with ASM2d model coupled with ACP precipitation. Both studies again support the idea that ACP was formed prior to HAP.

In this study, experiments were carried out with granular sludge in which HAP has been observed to accumulate in the core (Mañas et al., 2011). From literature it comes that HAP is not directly formed but precipitation is assumed to be controlled by precursor precipitation. The objective of this study is to investigate the operating conditions which can influence this first step of precipitation. Effect of pH is first evaluated in the biological reactor. Then precipitation tests are performed with the same granular sludge but in separate reactors which allow modeling the kinetic of precipitation of calcium phosphate. Contribution of precipitation in the granular sludge process will be then discussed in a next section, considering the influence of pH and biological reactions.

2. Materials and methods

2.1. Biological reactor operating conditions

Reactor kinetic tests were first carried out in two lab-scales continuously running Granular Sequenced Batch Airlift Reactor (GSBR), called R1 and R2 in what follows for simplicity. Details can be consulted in Wan et al. (2009) and Mañas et al. (2011). Most of the following results were collected on GSBR noted R2 which was operated in 4-hour cycles with anaerobic/aerobic conditions as follows: 15 min of feeding; 20 min of anaerobic reaction (nitrogen gas injection); 145 min of aerobic reaction; 30 min settling and 30 min withdrawal (with a volumetric exchange ratio of 47%). The synthetic feed had the following composition: 1000 mg/L COD consisting of a 25% each of glucose, acetate, propionic acid and ethanol contribution, nutrients and salts ($[PO_4^{3-}]$=30 mgP/L, $[Ca^{2+}]$=46 mg/L, $[HCO_3^-]$=100 mg/L, $[NH_4^+]$=50 mgN/L). A COD/N–NH_4^+ ratio of 20 was maintained. The reactor had a working volume of 17 L. The temperature was maintained at 20 ± 2 °C, and pH varied during the process cycle (from 7.2 to 8.5 on average). These last parameters, together with DO, were measured and recorded online for more than 250 days of the reactor operation. During this period, pH evolved naturally in the bulk under the influence of biological reactions (denitrification, nitrification) and physicochemical processes (CO_2 stripping, precipitation, etc). During this operation, three kinetic tests were followed at different pH values: (1) a normal cycle where pH was not controlled during the kinetic batch cycle, (2) a cycle at the high pH value of 8.4 ± 0.2 (by NaOH dosing), and (3) a cycle at the low pH value of 7.4 ± 0.2 (by NaOH and HCl dosing).

2.2. Batch precipitation in abiotic experiments

Batch tests were carried out in parallel to assess the precipitation of calcium phosphate from all of the P removal mechanisms separately (without biological reactions). For this purpose, a 2 L-volume reactor was seeded with aerobic granules from the GSBR-R2 reactor, and the kinetics was determined after an endogenous stage (sludge was aerated without feeding). The endogenous period depended on the test and the objective was to deplete the nutrients as far as possible at the kinetics starting point, ensuring a stable and low respirometric activity and stable evolution of ions in the bulk. At the end of the endogeneous period, pH was 8.15; and the ions concentrations were constant and as follows: $[Ca^{2+}]$=12.29 mg/L, $[PO_4^{3-}]$=2.94 mgP/L; $[Cl^-]$=171.58 mg/L, $[NO_2^-]$=4.66 mgN/L; $[NO_3^-]$=8.99 mgN/L, $[Na^+]$=237.97 mg/L, $[K^+]$=22.54 mg/L, $[Mg^{2+}]$=0.23 mg/L and $[NH_4^+]$=0 mgN/L. Calcium and phosphorus were added to the batch reactors at different amounts, maintaining a regime of constant mixing (260 rpm) and an air flow rate of 60 L/h. A pH and a DO probe were placed in the reactor and data were acquired online every 5 s (DO was stable at 6 ± 0.01 mg/L). All batch tests were performed at a temperature of 25 °C. No ammonium, magnesium or carbonates were added in the tests, in order to avoid the co-precipitation of other species and to limit the study to the calcium phosphate system. A different set of tests were carried out in order to evaluate the parameters reported to influence the precipitation mechanisms in the literature (pH, ionic strength, Ca/P concentrations, *VSS* and time).

All the experiments carried out in the physicochemical reactor can be classified in two sets including different periods (P0, P2, P3, etc.). Each set was performed at a different initial *VSS* concentration (S1=3.73 and S2=0.51 g/L) and, in each period, a change of a parameter (pH, I_c, [Ca], [P], Ca/P ratio, etc.) was studied. Table 1 summarizes the experiments performed. Ca and P concentrations were analyzed at different times for each experiment in order to evaluate the ΔCa/ΔP disappearing from the bulk, and experimental ratios were then compared to the theoretical ones for the minerals most likely to precipitate according to the *SI* calculation (see Section 2.4).

2.3. Characterization of liquid and solid samples

Then, samples were filtered with 0.2 μ-pore-size acetate filters before being analyzed by ionic chromatography (IC25, 2003, DIONEX, USA), in which NO_2^-, NO_3^-, PO_4^{3-}, NH_4^+, Ca^{2+}, K^+,

Table 1
Precipitation experiments in the 2 L reactor (batch) with different parameters.

Experiment	VSS_{init} (g/L)	TSS (g/L)	pH_{init}	pH_{mean}	I_{cinit} (10^{-2})	Ca_{init} (mg/L)	P_{init} (mg/L)	Ca/P_{init} (mol Ca/mol P)	Total duration (min)
S1P1	3.73	7.4	7.95	7.95	1.29	34.20	14.98	1.77	12
S1P2	3.73	9.6	6.83	6.86	2.32	86.01	114.20	0.58	280
S1P3	3.73	12.6	6.43	6.72	3.33	210.62	45.90	3.56	77
S1P4	3.73	15.8	6.71	6.62	3.39	89.34	104.83	0.66	7
S1P5	3.73	18.4	7.26	7.33	3.40	54.44	84.01	0.50	1173
S1P6	3.73	36.3	7.24	7.09	3.69	21.86	64.61	0.26	39
S2P1	0.51	2.66	7.78	7.77	1.20	33.40	14.27	1.81	1530
S2P2	0.51	2.86	7.77	7.30	1.77	71.10	32	1.72	467
S2P3	0.51	2.86	8.6	8.01	1.61	36.76	12.66	2.25	67
S2P4	0.51	2.86	9.17	8.77	1.60	22.73	8.49	2.53	15
S2P5	0.51	6.47	8.5	7.25	6.91	474.30	484.28	0.76	12
S2P6	0.51	6.47	6.5	6.48	5.71	92.32	315.54	0.23	31

Mg^{2+} concentrations were determined. COD, *MLSS* and *MLVSS* were analyzed according to standard methods (AFNOR 1994).

Solid samples were collected at the end of each batch of tests. Granules were separated from suspended particles by rapid settling (5 min). Granule samples and suspended solids were characterized separately. After calcination at 500 °C for 2 h, samples were analyzed by X-Ray Diffraction (XRD) (BRUCKER D5000), with a cobalt tube scattering from 4–70° in 2θ.

EDX analysis was performed with a photon X analyzer (Quantax Technology Silicon Drift) having a detection limit of 127 eV. It was coupled to a SEM (JEOL 5410 LV) which allowed working in a partial pressure chamber.

2.4. Calculation and modeling

The ionic strength (I_c) and supersaturation index (*SI*) of the minerals considered were calculated using the geochemical software PHREEQC (Parkhurst, 2000), with a modified database taking into account the pK_{sp} of the different minerals from the NIST database (2011) at the temperature at which the tests were conducted (25 °C).

A dynamic model was developed to predict calcium phosphate precipitation based on differential equations as described in Annex 1 written in the form of a *Petersen* matrix. The model was solved with AQUASIM software. Based on the work of Musvoto et al. (2000a and 2000b), the model included acid-base reactions and ion pair formation, described by a combination of the forward and reverse reactions of dissociation. Selection of ion pair species was based on exhaustive species decomposition with the PHREEQC software (Minteq v4 database, modified). For a more accurate prediction of phosphorus concentration in solution, two ion pairs containing phosphorus were added to the dynamic model proposed by Musvoto: MgH_2PO_4 and $NaHPO_4$. Both softwares were used successively. PHREEQC software allows first to decompose the concentrations obtained from the experimental analysis with ion chromatography (total calcium, magnesium, phosphorus, etc…) into aqueous species and ion pairing complexes. The output values of PHREEQC serve as inputs for initializing the differential equations described in AQUASIM, ensuring a better accuracy of the results (otherwise the dynamic simulations initially show an equilibrium period of a few minutes).

Precipitation equation for the precursor was described using the nomenclature of Koutsoukos et al. (1980), according to the following equation:

$$\frac{d}{dt}M_{v+}A_{v-} = K_{MA}[((M^{m+})^{v+}(A^{a-})^{v-})^{1/v} - (10^{-pK_{sp-MA}})^{1/v}]^n \quad (1)$$

where $M_{v+}A_{v-}$ represents the soluble salt, ACP (or TCP) in this case; K_{MA} is the kinetic constant; (M^{m+}) and (A^{a-}) are the ion activities; $v+$ and $v-$ are the number of cationic and anionic species, respectively, $(v = v+v-)$ in the salt; n is the number of different ion species in the salt; and pK_{sp-MA} is the negative log value of the dissociation constant. As precipitation is a surface limited reaction, the kinetic constant is dependent on the amount of solids present in the system. It was fitted to the experimental data for each assay. The pK_{sp-MA} is the thermodynamic constant and it is specific to the mineral phase and the given temperature. It is normally provided in the literature.

SI for each mineral considered was calculated according to the Eq. 2, which considers the term j (in contrast with default calculation with PHREEQC®), which is the number of ions contained in the mineral formula considered (Paraskeva et al., 2000; Monstastruc, 2003).

$$SI = \log\left(\frac{IAP}{K_{sp}}\right)^{1/j} \quad (2)$$

where *IAP* is the Ionic Activity Product of the ion activities involved in the mineral precipitation, and K_{sp} refers to the thermodynamic mineral precipitation constant at a given temperature. Values were thus compared to 0, being probable to precipitate those minerals whose *SI* were positive in the bulk. Ionic coefficients are calculated according Davies expression (Loewenthal et al., 1989):

$$\log f_i = -AZ_i^2\left(\frac{{I_c}^{1/2}}{1+{I_c}^{1/2}} - 0.3I_c\right) \quad (3)$$

$$I_c = \frac{1}{2}\sum C_i Z_i^2 \quad (4)$$

$$A = 1.825 \times 10^6 (78.3T)^{-1.5} \quad (5)$$

where f_i is the activity coefficient for ionic species, (f_m, f_d or f_t), monovalent, divalent or trivalent, respectively; I_c, is the ionic strength in the solution; A, is the temperature-dependant constant; C_i, is the concentration of the ith ionic species (in mol/l); Z_i, is the charge of the ith ionic species; T, is the temperature (in Kelvin).

A simplified version of the physico-chemical model is provided in Annex 1, where CO_2 stripping and NH_3 expulsion were also considered according to the following equations:

$$[H_2CO_3^*] = [CO_2 \text{ dissolved}] + [H_2CO_3] \quad (6)$$

$$\frac{d}{dt}[H_2CO_3^*] = \left(\frac{D_{CO_{2(g)}}}{D_{O_2}}\right)^{0.5} Kla_{O_2}(K_{H,CO_{2(g)}} \times \rho_{CO_{2(g)}} - [H_2CO_3^*]) \quad (7)$$

$$\frac{d}{dt}[NH_3] = Kla_{NH_3} \times (-[NH_3]) \quad (8)$$

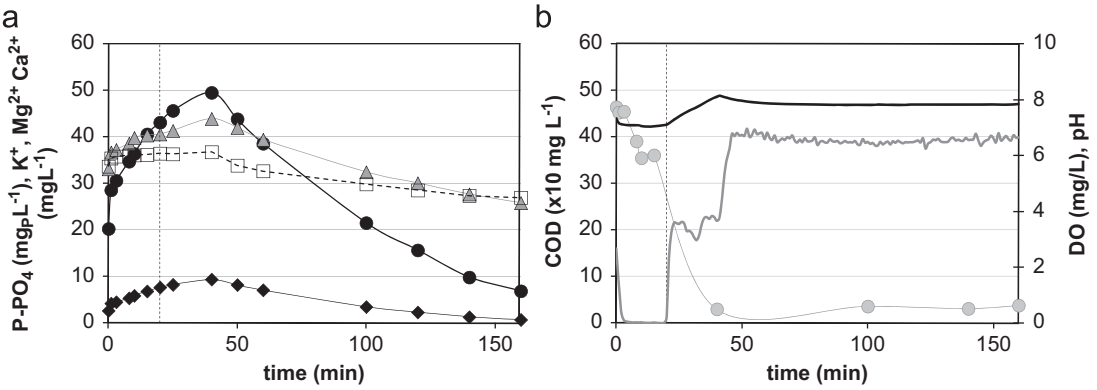

Fig. 1. Kinetic cycle in GSBR (R2) operated at normal conditions (without pH control). (a) Evolution of PO_4^{3-} (●), Ca^{2+} (□), Mg^{2+} (♦), K^+ (▲); (b) COD (◯), pH (—) and DO (—) during a cycle run.

where $\rho_{CO_{2(g)}}$ is the partial pressure of CO_2 and K_{H,CO_2} is the Henry's law constant for CO_2. For the stripping of NH_3, the partial pressure of this gas is neglected. Only expulsion of NH_3 is considered in the model. DCo_2 and DO_2, are the liquid diffusion constants for CO_2 and O_2, respectively.

3. Results

3.1. Ca and P behavior in the biological reactors: influence of pH

Under normal operating conditions (Fig. 1), two successive stages were observed during the GSBR cycle. First K^+, Mg^{2+} and PO_4^{3-} were released during the anaerobic phase, whereas calcium was nearly constant (slight increase). During this phase, polyphosphate accumulating organisms (PAOs) consumed volatile fatty acids (a fraction of the COD) at the expense of energy release by the breakage of intracellular polyphosphate, composed of K^+, Mg^{2+} and PO_4^{3-} (Jardin and Pöpel, 1996; Barat et al., 2005). Then, in the subsequent aerobic phase, phosphorus was taken up by the PAOs, thus reconstituting the polyphosphate source and resulting in a net phosphorus removal from the bulk at the end of the aerobic cycle. Fig. 1b also shows the pH profile during the course of the cycle: pH first slightly decreases during anaerobic phase due to proton release (as observed by Serralta et al., 2004) and then increased to 8.2 at the beginning of the aerobic period due to CO_2 stripping. At the end of COD consumption, aerobic respiration declined and pH decreased. This could be explained by proton release during biological nitrification and also a possible acidification can be due to calcium phosphate precipitation. Calcium remained constant during the pH plate profile and then decreased, the decrease coinciding with the maximum phosphate concentration in the bulk.

Simultaneous storage of a part of the phosphates from the bulk occurred in the form of calcium phosphate precipitates inside biological granules, demonstrated by SEM-EDX analysis (Fig. 2). A Ca:P molar ratio of 1.64 ± 0.09 was found in the mineral core which is close to that of HAP ratio (1.67). Our precedent study based on different analytical techniques (Raman, EDX, X-ray diffraction) had proven that HAP was the major mineral (Mañas et al., 2011). This second mechanism contributing to phosphorus removal and immobilization is noted as Microbial Induced Phosphorus Precipitation (MIPP).

Three experiments were carried out in the biological GSBR, two with pH controlled at 8.4 ± 0.2 and 7.4 ± 0.2, and another at the normal pH evolution Calcium and phosphate profiles in the supernatant are shown in Fig. 3a and b respectively. Initial examination suggested that pH strongly influenced the phosphate profile (Fig. 3b). Experiments at high or low pH both led to a

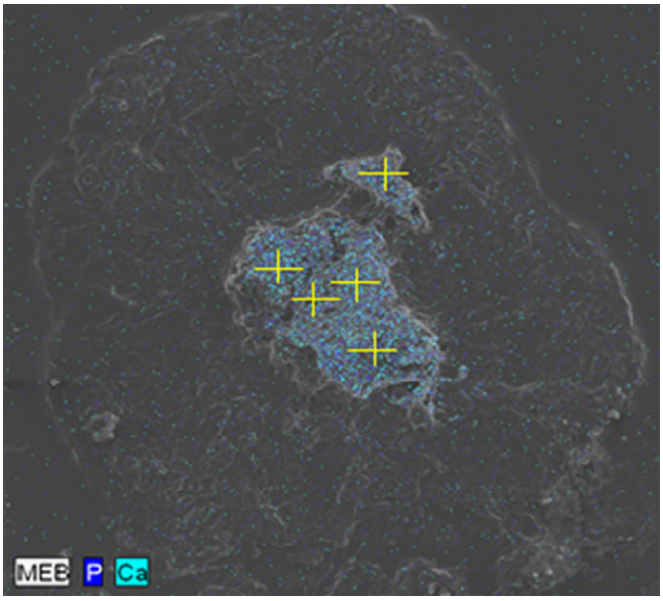

Fig. 2. Granule cut analyzed with SEM-EDX analysis showing calcium phosphate inside.

decrease of the phosphate release and uptake. A better P removal yield was finally achieved when pH was not controlled. A first reason is probably that micro-organisms (PAOs) are disturbed by a sudden change of pH in the reactor (here the final pH was 0.5 units higher or lower than in the normal cycle). A second explanation may be that precipitation is favored at high pH, masking the EBPR process. Given that two processes (MIPP and EBPR) are responsible for the total phosphate behavior, the contribution of precipitation could be evaluated with respect to calcium removal. The higher the pH in the bulk, the lower the calcium concentration obtained, strengthening the contribution of precipitation to the whole process.

Fig. 4 shows the variation of calcium concentration versus pH, obtained from different kinetics carried out at different moments during the running period. We extended the analysis to two GSBRs: R1 (operated in anoxic/aerobic conditions) in which pH reached higher values induced by a higher denitrification activity, and R2 (operated in anaerobic/aerobic conditions). Fig. 4a compares the effect of pH induced biologically in two reactors, GSBR R1 and R2. The details of the first reactor will not be given here but the main difference with respect to R2 relies in the introduction of an anoxic phase (with the presence of nitrate as an electron acceptor) instead of the anaerobic one of R2. Thus, in R1, biological denitrification induced

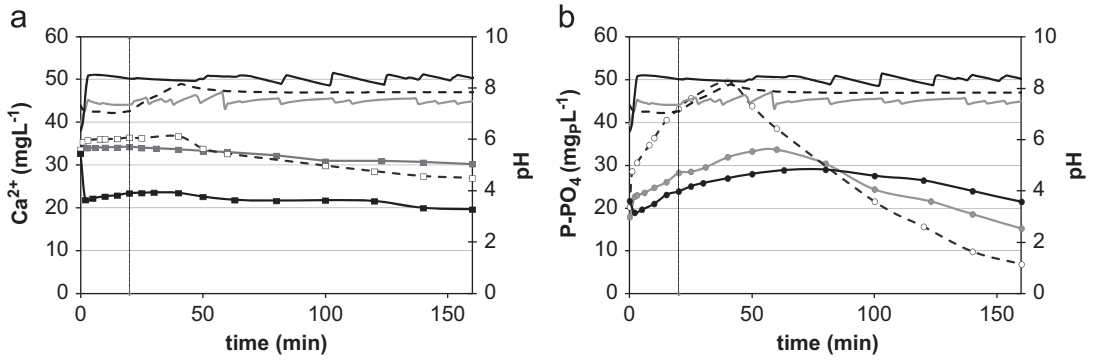

Fig. 3. Kinetic tests in biological reactor at different pH (a) calcium and pH; and (b) phosphorus and pH. Legend: Ca(□), P (○), pH(-); normal kinetics (black, dotted line); high pH (black); low pH (gray).

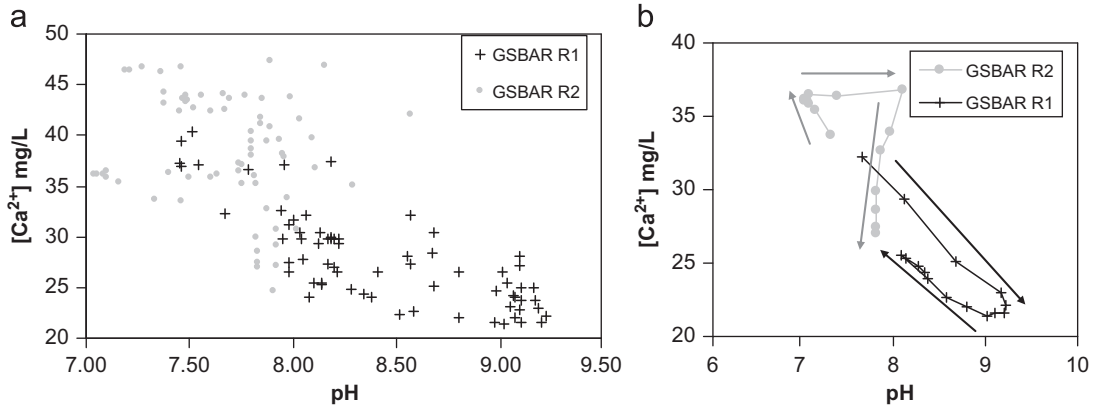

Fig. 4. Calcium concentration versus pH in two biological GSBR: (a) set of points corresponding to different kinetics during the reactor running period and (b) comparison of the tendency of calcium profiles with pH during a kinetic course in both reactors.

Table 2
Supersaturation indexes with respect to different minerals in the bulk at the beginning of the batch precipitation tests calculated with PHREEQC at $T=25$ °C.

Supersaturated solid phases calculated by PHREQC											
Test	**HAP**	**ACP**	**HDP**	**TCP**	**OCP**	**DCPD**	**DCPA**	**CAL**	**ARAG**	**NEW**	**$Mg_3(PO_4)_2$**
S1P1	1.28	0.57	0.05	1.31	−5.43	−0.18	−0.04	−0.87	0.11	−1.62	−1.79
S1P2	1.06	0.45	−0.22	1.19	−5.40	0.20	0.34	0.29	−0.38	−1.29	−1.97
S1P3	1.81	1.03	0.54	1.77	−4.88	−0.24	−0.10	0.60	0.51	−1.04	−0.57
S1P4	1.02	0.40	−0.26	1.14	−5.48	0.17	0.31	−0.39	−0.48	−1.01	−1.64
S1P5	1.19	0.54	−0.10	1.28	−5.32	0.13	0.27	−0.19	−0.28	−0.97	−1.41
S1P6	0.92	0.25	−0.29	1.00	−5.80	−0.13	0.02	−0.39	−0.48	−1.16	−1.62
S2P1	1.18	0.48	−0.03	1.22	−5.55	−0.20	−0.06	−1.00	−0.03	−1.26	−1.44
S2P2	1.43	0.75	0.13	1.49	−5.07	0.09	0.23	−0.88	0.10	−1.04	−1.24
S2P3	1.52	0.77	0.28	1.51	−5.21	−0.24	−0.10	−0.60	0.38	−1.20	−1.02
S2P4	1.59	0.80	0.39	1.54	−5.27	−0.44	−0.30	−0.43	0.55	−1.33	−0.91
S2P5	2.26	1.64	0.76	2.38	−3.65	0.73	0.87	0.72	0.63	−1.59	−0.87
S2P6	0.98	0.38	−0.31	1.13	−5.44	0.28	0.42	−0.58	−0.67	−0.84	−1.72

higher pH increase (from 7.5 to 9.2) than in R2, resulting in a higher contribution of the precipitation phenomenon. Fig. 4b shows that, when pH increases to 9 in R1 (at the end of anoxic phase), calcium concentration decreases in the bulk as a consequence of precipitation, reaching the lowest value observed (around 22 mg Ca/L). Meanwhile, there is calcium release when the pH decreases. The same figure for R2 shows a different trend: calcium concentration increase is followed by a flat stable period during which pH increases (until the end of phosphate release by PAO), then calcium decreases during the aerobic phase, probably due to precipitation. At the end of the cycle, calcium concentration reaches a similar value (25–26 mg/L) in both reactors, as final pH values are also similar (7.9–8). Finally these data point out the important influence of the biological reaction on pH and its consequences on precipitation.

3.2. Calcium precipitation in the batch tests

In order to assess the calcium precipitation kinetics separately from EBPR reactions, batch tests were performed individually with sludge samples maintained aerated and mixed in endogenous conditions. Various pH, ionic strengths, *TSS* and initial calcium and phosphorus concentrations were tested. Simulations with PHREEQC software considering the supernatant quality at the starting point of each test indicated the minerals that were supersaturated in the bulk ($SI > 0$ in Table 2).

In all tests, hydroxyapatite (HAP), amorphous calcium phosphate (ACP) and tricalcium phosphate (TCP) were systematically supersaturated in the bulk. Aragonite, which is one of the polymorphs of calcium carbonate, was only thermodynamically

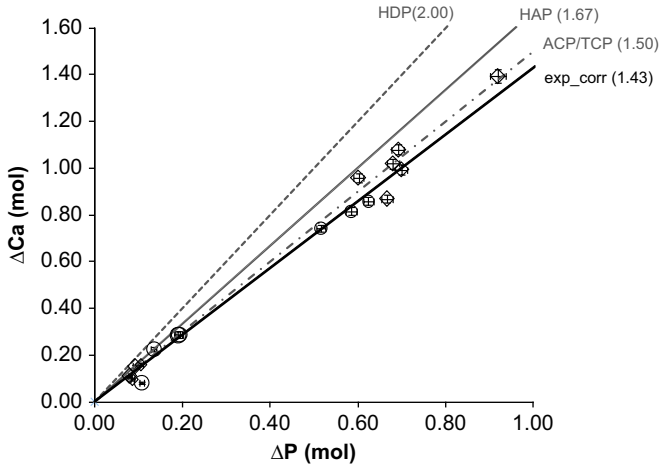

Fig. 5. Experimental ΔCa versus ΔP (mmol) precipitated in the batch tests, compared to the reference ratios for minerals that were supersaturated in the bulk.

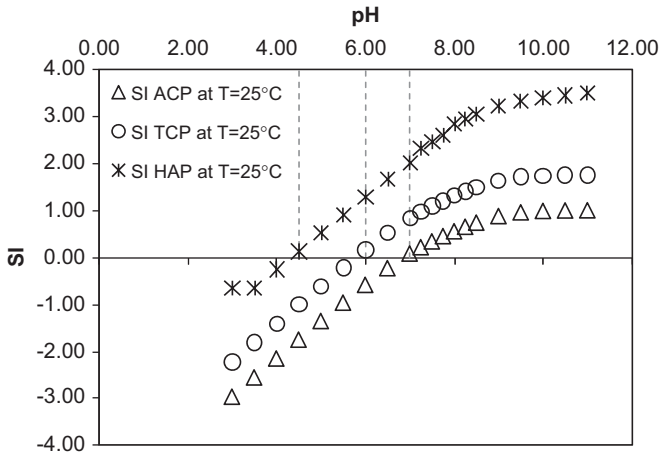

Fig. 6. pH influence on ACP, TCP and HAP supersaturation index calculated by PHREEQC® for test S2P1.

susceptible to form in tests with high pH and low *VSS*, or initially at high *VSS* concentration, when inorganic carbon was not already depleted. Neither octacalcium phosphate (OCP), nor newberite (NEW) and nor magnesium phosphate were supersaturated in the bulk. Brushite (DCPD), phosphate dicalcic anhydrous (DCPA) and hydroxidicalcium phosphate (HDP) were only supersaturated for some of the tests (the latter, coinciding with aragonite saturation).

Only the batch tests in which pH values coincided with the range of pH observed in the GSBR (6.5–9.1) were considered for evaluating Ca:P stoichiometry. Fig. 5 shows the variation of calcium versus phosphate, indicating the experimental Ca:P stoichiometry in the different tests. For each point, relative standard deviation was 2.5% (mainly due to ionic chromatography analysis). The sets of experiments were correlated to a straight line, the average slope of which gave a Ca:P ratio of 1.43 ± 0.03.

It can be seen that most of the points are arranged in a row close to that of the theoretical mineral ACP/TCP (Ca:P=1.5), indicating that the last two phases are the most likely to precipitate prior to HAP crystallization in the different conditions tested. No significant influence of pH (range 6.5–9.1), calcium and phosphorus concentrations (range 20–300 mg/L) or ionic strength (range 1.2×10^{-2}–5.7×10^{-2}) was found on this ratio. Since ACP and TCP have the same molar Ca/P ratios, the above methodology does not distinguish between the two minerals. Considering the fact that pH could vary between 6.5 and 9 in a biological reactor, Fig. 6 shows the influence of pH on the *SI* of the three major supersaturated phases according to PHREEQC: ACP, TCP and HAP. Simulations were conducted with the concentrations corresponding to experiment S2P1, comparable to those in the range measured in the biological reactor (33 mg/L for Ca and 14 mg/L for P).

Table 3
Thermodynamic precipitation constants of ACP and TCP from the literature.

Mineral phase	pK_{sp} (T=25 °C)	Reference
ACP	25.46	Hoffmann, 1977
	26.52	Seckler et al., 1996
	25.2	Meyer and Weatherall, 1982
	28.92	NIST database, 2011
(β)-TCP	32.63	Murray and May, 1996
	32.7	NIST database, 2011
	28.77	Song et al., 2001

The *SI* of the minerals increased proportionally to the pH in the bulk, revealing for all of them, one pH value at which HAP, then TCP and finally ACP started to become supersaturated, the other parameters remaining constant. Since the Ca:P ratios of ACP and TCP were similar due to the similarities in their chemical formula, modeling was further evaluated to isolate the most probable precursor driving HAP crystallization in aerobic granules.

3.3. Modeling calcium phosphate precipitation

Based on the batch tests, three experiments (S2P1 and S2P2 at low *VSS* concentration, and S1P5 at high *VSS* concentration) were modeled using AQUASIM software, combined with PHREEQC for the initial conditions. The kinetic constant rate of the mineral (K) and the thermodynamic constant were fitted in the model as the values proposed for the last one in literature vary widely according to the different authors (Table 3).

Fig. 7 shows the calcium and phosphorus profiles modeled in the aforementioned tests compared to the experimental points. The adjusted model matches the experimental data well, and the kinetic constants together with the pK_{sp} fitted for each experiment are shown in Table 4. Results show that the higher the *TSS* concentration in the bulk, the higher the kinetic constant rate of precipitation. In contrast, pK_{sp} values were very similar in all the experiments. An average value of p$K_{sp}=28.07 \pm 0.58$ was obtained. Considering a single pK_{sp} for all the experiments, a satisfactory pK_{sp} value was obtained from the mean of the previously fitted values, allowing the thermodynamic constant of the precursor phase to be found.

The sensitivity of the model to pK_{sp} value is evaluated in Fig. 8. The three sets of tests chosen were modeled taking 3 different pK_{sp} values into account according to Table 3: the minimum provided in the literature (25.2), the maximum provided (32.63) and the mean value calculated above from the experiments modeled (28.07).

It can be seen that the model (with a p$K_{sp}=28.07 \pm 0.58$) described the observations correctly for different initial Ca:P ratios.

3.4. Analysis of the solid phases

Precipitates were collected and analyzed at the end of each experimental series and were representative of the cumulated mineral matter in the 2 L reactor.

Fig. 9 shows the XDR analysis conducted on two samples: the suspended matter precipitated (black), and the sample of biological granules. Both samples were compared to the most coincident

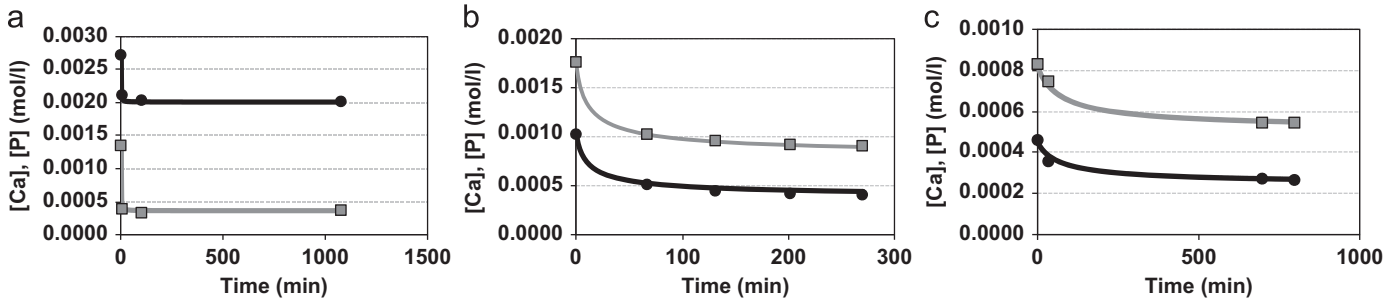

Fig. 7. Comparison of experimental and modeled assays at different *MLSS* concentrations: (a) 18.4 g/L; (b) 2.66 g/L; and (c) 2.86 g/L. Legend: [Ca] in gray; [P] in black.

Table 4
Thermodynamic precipitation and kinetic rate constants deduced from the model.

Assay	*TSS* (g/L)	pK_{sp} value	Kinetic constant rate (min^{-1})
S1P5	18.40	28.36	3.81×10^7
S2P1	2.86	27.99	4.13×10^5
S2P2	2.66	27.88	1.16×10^5

mineral patterns in the database of the software used (EVA®). The XRD spectra highlighted two coincident patterns with clear individual peaks: hydroxyapatite (HAP) and sylvite (KCl). Sylvite (KCl) was only observed in the suspended matter. It is a very soluble salt which was certainly not precipitated in the reactor initially but was formed during the evaporation of the sample (the presence of K^+ and Cl^- in the solution was due to the potassium phosphates and calcium chloride used for batch tests).

The HAP spectrum was the one that explained the major peaks for both granules and suspended solids samples. In addition, the spectra indicated the probable presence of amorphous phases, which could explain the large peaks that do not exactly match any crystalline forms.

The most important conclusion is that both sample patterns match and coincide with that of HAP almost perfectly, despite the black peak at 33°, 47° and at 58° in the 2θ abscissa axis, which corresponds to that of the sylvite mentioned above. Another conclusion is that, whatever the precursor is, the final phase crystallized seems to be HAP, both in the bulk and in the granules, and that the time scale for its precipitation is less than 7 days. These results confirm the similarities between the precipitated phases found in the supernatant during the batch tests and those observed inside the granules.

4. Discussion

4.1. ACP: the precursor of HAP in granular sludge processes

The results globally confirm that HAP is the major crystallized mineral accumulated in the granular sludge in the long term. But data also indicate that calcium phosphate precipitated first during each batch cycle, due to super-saturation in a precursor form which was probably ACP. According to House and Donaldson (1986), HAP precipitation crystallizes through a precursor when heterogeneous nucleation takes place, which was the case here. Although different precursors are proposed in the literature, ACP seems to be the one that can be formed at a wider pH range, and different ionic strengths. Results obtained in this paper for the precipitation batch tests (in which biological activity was limited), led to a calcium phosphate precursor with Ca:P molar ratios between 1.38 and 1.59, with a mean value of 1.43 ± 0.03, which fits with ACP. Modeling different assays at different *MLSS* concentrations revealed that the pK_{sp} that best fitted the data was $pK_{sp25\ °C} = 28.07 \pm 0.58$. The thermodynamic constant was compared to that provided in the literature (Table 3) and corresponds to ACP for the NIST database, whereas TCP, which is also supersaturated in the bulk should theoretically present a higher pK_{sp}. Regarding the precursor phases able to form in acidic conditions (Gao et al., 2010), neither brushite (DCPD), nor monetite (DCPA) and nor octacalcium phosphate (OCP) were likely to form in the biological reactor from a thermodynamic point of view, considering the *SI* negative values This result first contrasts with the model by Maurer and Boller (1999), proposed the HDP as a precursor form, with Ca:P molar ratio = 2. In our work, the only test in which the Ca:P removal ratio was close to 2 could be explained by a simultaneous precipitation of calcium carbonate, which is supported by the supersaturation index (*SI*) calculated with PHREEQC (see Table 2). Thus, our results confirm the approach of Barat et al. (2011) and Musvoto et al. (2000a and 2000b) considered ACP as the first step of calcium phosphate precipitation.

Finally, modeling ACP formation by the Koutsoukos et al. (1980) model predicted calcium and phosphate behavior during the batch tests quite well. These assays were predicted only for the short term (from 3 to 15 h) and it should be noted that the progressive formation of HAP should also be included in the long term as it was demonstrated to accumulate after several days.

4.2. Operating pH conditions influencing MIPP in GSBR

Supersaturation with respect to Ca, P concentrations and pH, are the major parameters that influenced precipitation. In order to evaluate how pH drives calcium phosphate precipitation, Fig. 10 shows the evolution of calcium concentration as a function of pH, obtained by modeling different pH values over different kinetics during the running period in order to assess the contribution of P precipitated with calcium at each pH in equilibrium. Simulations were carried out using the model described above, which allowed the calculation of the equilibrium concentration for Ca^{2+} and PO_4^{3-} at the different pHs tested between 6.5 and 9.5. Different Ca:P ratios and initial concentrations were tested in the influent, in order to assess the limiting conditions for the maximum P removal fraction by precipitation (in the case that no biological P removal takes place).

The results in Fig. 10 pointed out that in the current influent conditions ([Ca] = 50 mg/L and [P] = 30 mg/L), the maximum fraction of P that could be removed by precipitation achieves the 55% at final pH = 8. This is under the assumption that no interference with EBPR process took place. Indeed in the bioreactor, experimental kinetics showed a higher P removal but a lower contribution of the precipitation mechanism (39.6%), which is due to simultaneous biological P removal (EBPR). Fig. 10b confirms that pH seriously influences the Ca–P precipitation: variation of one pH unit from 7.5 to 8.5 leads theoretically to an increase P removal from 40% to 75%, at the GSBR working pH range.

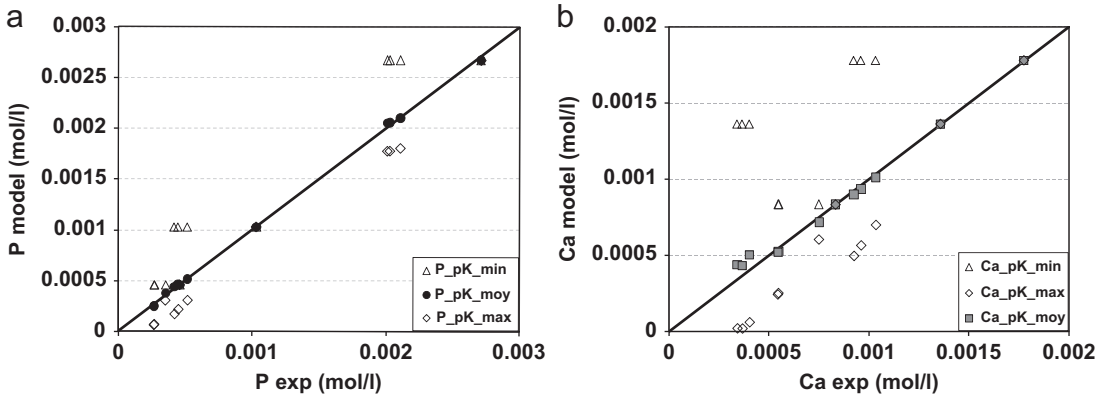

Fig. 8. Model sensitivity to the different precipitation constants (pK_{sp}) (a) [P] prediction; and (b) [Ca].

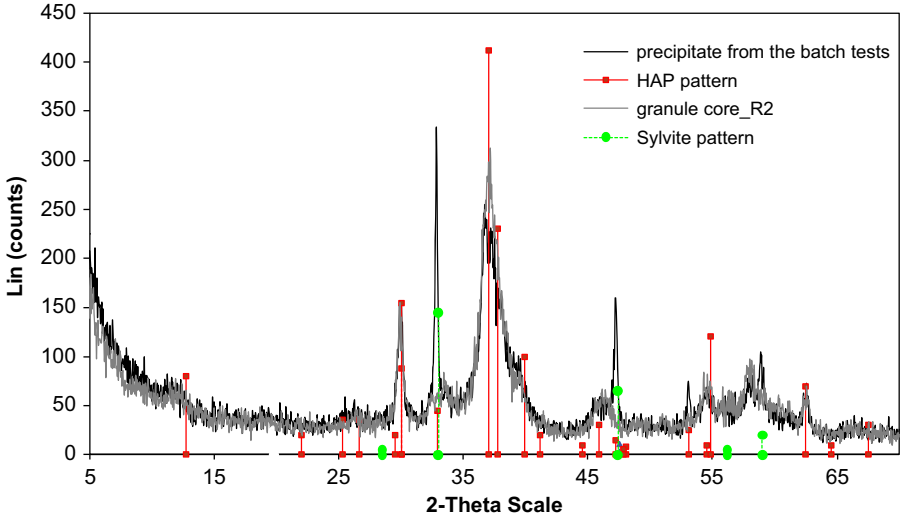

Fig. 9. Comparison of the mineral precipitated at the end of the batch tests and mineral fraction in the core of biological granules.

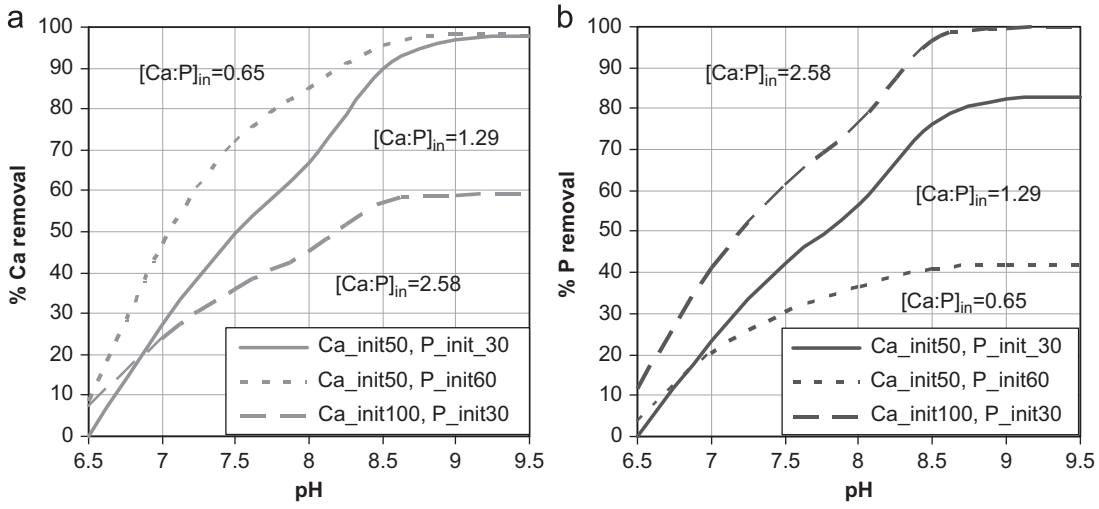

Fig. 10. Contribution of calcium phosphate precipitation within different pH attained at the end of each kinetic phase in the GSBR. Ca:P ratios in the inlet are in mol. (a) % of Ca removed by precipitation (gray) and (b) % of P removed by precipitation (black).

Therefore, P removal by Ca–P precipitation can vary a lot depending on the final pH attained at the end of the cycle. For example 25% of phosphorus could precipitate for a pH of 7 whereas about 85% of phosphate would precipitate for a pH of 9. As indicated in Fig. 10, precipitation was observed in the sequencing batch reactor due to an enough level of calcium and phosphate achieved in the influent (50 mg/L of Ca and 30 mg/L of P). The amount of calcium–phosphate formed in the reactor is first driven by the amount of calcium and

phosphate present in the bulk. Finally, Fig. 10 also shows how the amount of P removed by precipitation increased as the influent Ca/P ratio increases.

4.3. Influence of biomass and bioreactions on precipitation

The precipitation process is also influenced by biomass in different ways: (1) bio-aggregates play a catalyzing role at the nucleation sites, (2) some of the bioreactions modify the pH locally and transiently, and (3) some of the bio-reactions transiently release phosphates (coming from internal polyphosphate).

Identification of the model parameters indicated that the kinetic rate of calcium phosphate precipitation increased with suspended solids concentration. Obviously, it is well known that precipitation is a surface controlled process and the differences in the values of the kinetic constants can be linked to the surface available for crystal nucleation. Moreover no precipitates were observed in batch tests without any sludge addition ($VSS=0$, results not shown) whereas crystal formation was observed in tests with even lower initial Ca and P concentrations and even lower pH but previously seeded with microbial aggregates, leading to the conclusion that heterogeneous nucleation onto the suspended biological aggregates should constitute a first step towards the MIPP process. Fig. 11 shows different images of microscopic observations over the different experiments in the batch reactor.

At the end of a normal cycle in the bioreactor, no crystals were found in the supernatant (Fig. 11a). In contrast, in the batch assays, nucleation began (Fig. 11b) and some crystals started appearing on the bioaggregates' interface (Fig. 11c). Different crystallization forms were observed during the physicochemical tests (Fig. 11d, e and f), all converging in dendritic crystals centered in rhombohedral structures that finally superposed to form rectangular terraces like the HAP formation reported by Chakhmouradian and Mitchell (1999), Elliott (1994).

As calcium phosphate in the form of HAP was observed in the center of granules, it is likely to think that bioreactions could locally increase the supersaturation either by a pH increase or an

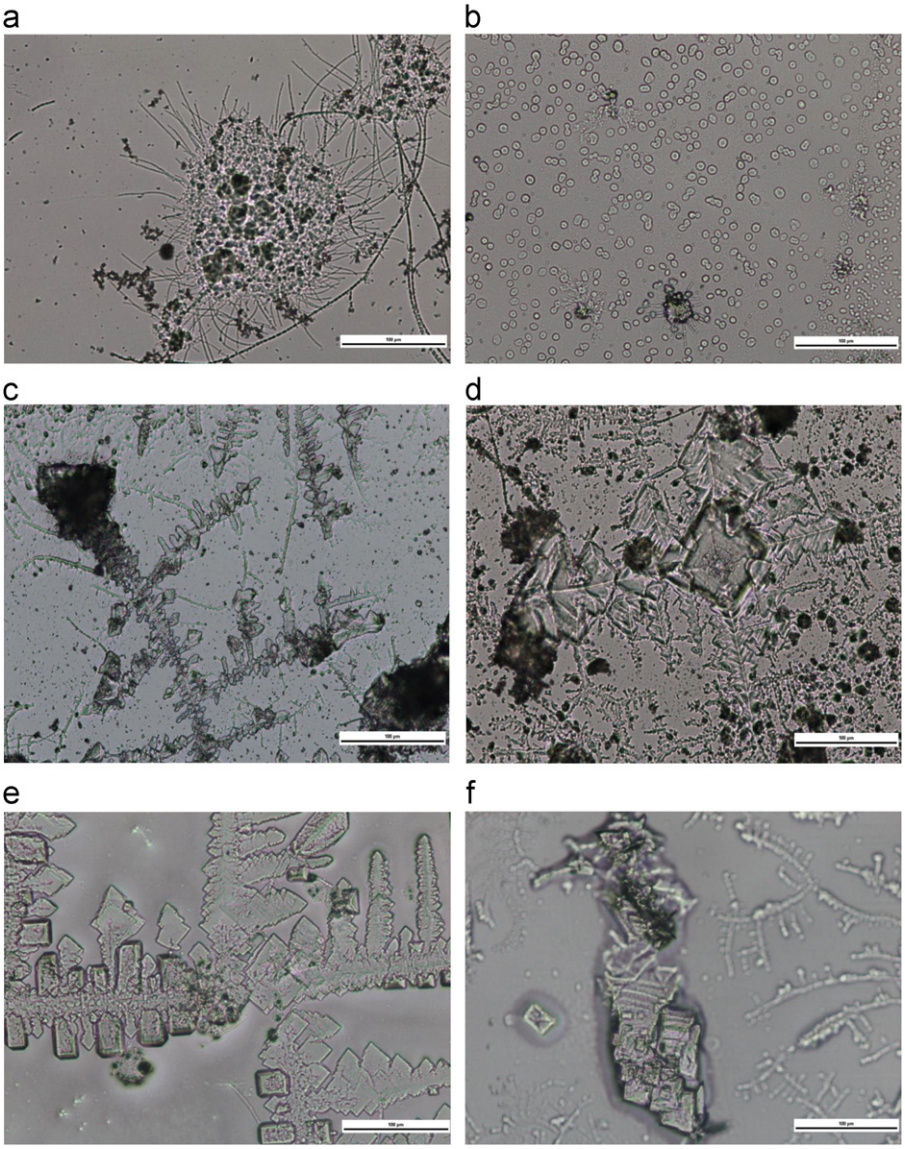

Fig. 11. *Mineral precipitation in the batch tests at different periods (scale bar=100 μm)*: (a) at the end of the aerobic period in the biological reactor; (b) beginning of the batch test with low *VSS* concentration; (c) dendritic growth of precipitates that have nucleated on organic sludge filaments; (d) rhombohedral shape of calcium phosphate growing at the crossing point of the dendritic crystals; (e) illustrates a co-precipitation of another phase onto the previous crystals and (f) shows the final helicoidal crystal growth of presumed HAP.

anaerobic phosphate release. In the beginning of the GSBR cycle when pH starts to increase due to denitrification (and also acetate consumption) and when P is released by PAO, heterogeneous nucleation of ACP probably begins on the surface walls of bacteria and maybe also in the internal pore of aggregates where anoxic or anaerobic activities are the most important. Partial solubilization of ACP at the surface of the bioaggregates could also take place during subsequent aerobic period as the nitrification provokes a proton release. On the other hand, the pH in the center could be maintained relatively high due to oxygen limitation favoring simultaneous denitrification, and amorphous calcium phosphate could be progressively converted to HAP in the core of granules. ACP cannot be detected by XRD (Banu, 2005), so no peaks of the precursor could be observed in the core of granules, only those of the crystallized HAP have been demonstrated. However, previous analysis with EDX probes showed that Ca and P content in the external part of bioliths was lower than those measured in the center (Mañas et al., 2011). Thus, HAP would probably crystallize with time and grow in an organic confined medium that would store it as a stable phosphate resource until granule breakage or purge.

5. Conclusions

In this work, experiments were conducted to investigate calcium phosphate precipitation in an EBPR process with granular sludge. Short term calcium phosphate precipitation was characterized by a Ca:P stoichiometry of 1.43 ± 0.03 which is close to those of ACP or TCP. Calcium and phosphate behavior were successfully modeled considering a mean pK_{sp} value adjusted to 28.07 ± 0.58, which is in accordance with the literature and comparable to that of ACP. After several days, amorphous calcium phosphate was converted to HAP, which was detected by XRD analysis.

The contribution of P removal by precipitation, which is linked to the MIPP mechanism responsible of the phosphate bioliths found in granules, is basically influenced by pH and Ca and P concentrations. In the conditions tested, a maximal contribution of precipitation between 40% and 75% of the P removed could take place depending on the final pH achieved in the biological reactor.

The presence of biomass influenced calcium phosphate precipitation in different ways: heterogeneous precipitation took place on bio-aggregates which formed the nucleation site, and the kinetic rate is hence proportional to suspended solid concentration (no signs of precipitation were found in the test carried out without biomass). Bioreactions that produce alkalinity, (example: denitrification) encourage precipitation in the bioreactor and also probably in the core of microbial granules, where hydroxyapatite is observed to accumulate. Future work will be necessary to investigate the slow conversion of amorphous calcium phosphate (ACP) to hydroxyl-apatite (HAP) occurring within the granules.

Nomenclature

ACP amorphous calcium phosphate [$Ca_3(PO_4)_2 \cdot xH_2O$]
ARAG aragonite [$CaCO_3$]
C (mg/L) concentration
COD (mg/L) chemical oxygen demand
DCPA dicalcium phosphate anhydrous, Monetite [$CaHPO_4$]
DCPD dicalcium phosphate dihydrate, Brushite [$CaHPO_4 \cdot 2H_2O$]
DO (mg/L) dissolved oxygen
EBPR enhanced biological phosphate removal
EDX energy dispersive X-ray analysis
GSBR granular sequenced batch airlift reactor
HAP hydroxyapatite [$Ca_5(PO_4)_3(OH)$]
HDP hydroxyl dicalcium phosphate [$Ca_2HPO_4(OH)_2$]
IAP ionic activity product
I_c (mol/Kg) ionic strength
K_{H,CO_2} Henry's law constant for CO_2
K_{sp} constant solubility product
MIPP Microbial Induced Phosphorus Precipitation
$MLSS = TSS$ (g/L) Mixed Liquor Suspended Solids/Total Suspended Solids
$MLVSS = VSS$ (g/L) (Mixed Liquor) Volatile Suspended Solids
NEW newberite [$MgHPO_4 \cdot 3H_2O$]
OCP octacalcium phosphate [$Ca_8H_2(PO_4)_6 \cdot 5H_2O$]
PAO Polyphosphate Accumulating Organisms
$rHAP$ (mol L^{-1} min^{-1}) rate of HAP precipitation
SEM Scanning Electron Microscopy
SI Supersaturation Index
T (°C) temperature
TCP (beta) tricalcium phosphate [$Ca_3(PO_4)_2$]
VSS (g/L) Volatile Suspended Solids
XRD X-ray diffraction
Ω degree of supersaturation

Acknowledgments

The authors would like to thank E. Mengelle, M. Bounouba, D. Delagnes, D. Auban, L. Montastruc, S. Julien and S. Becker for their help and contributions to this work.

Annex 1. Supporting information

Supplementary data associated with this article can be found in the online version at doi:10.1016/j.ces.2012.01.009.

References

Abbona, F., Lundager Madsen, H.E., Boistelle, R., 1986. The initial phases of calcium and magnesium phosphates precipitated from solutions of high to medium concentrations. J. Cryst. Growth 74 (3), 581–590.
Banu, M., 2005. Mise en forme d'apatites nanocristallines: ceramiques et ciments. Ph.D. Thesis. INP, Toulouse.
Barat, R., Montoya, T., Seco, A., Ferrer, J., 2011. Modelling biological and chemically induced precipitation of calcium phosphate in enhanced biological phosphorus removal systems. Water Res. 45 (12), 3744–3752.
Barat, R., Montoya, T., Seco, A., Ferrer, J., 2005. The role of potassium, magnesium and calcium in the Enhanced Biological Phosphorus Removal treatment plants. Environ. Technol. 26 (9), 983–992.
Bazylinski, D.A., 1996. Controlled biomineralization of magnetic minerals by magnetotactic bacteria. Chem. Geol. 132 (1-4), 191–198.
Benzerara, K., Miot, J., Morin, G., Ona-Nguema, G., Skouri-Panet, F., Férard, C., 2011. C. R. Geosci. 343, 160–167.
Boskey, A.L., Posner, A.S., 1974. Magnesium stabilization of amorphous calcium phosphate: a kinetic study. Mater. Res. Bull. 9 (7), 907–916.
Brown, W.E., Matthew, M., Tung, M.S., 1981. Crystal chemistry of OCP. Prog. Cryst. Growth Charact. 4, 59–68.
Chakhmouradian, A.R., Mitchell, R.H., 1999. Niobian ilmenite, hydroxylapatite and sulfatian monazite. Alternative hosts for incompatible elements in calcite kimberlite from international Naya, Yakutia. Can. Mineral. 37, 1177–1189.
De-Bashan, L.E., Bashan, Y., 2004. Recent advances in removing phosphorus from wastewater and its future use as fertilizer (1997–2003). Water Res. 38 (19), 4222.
Dupraz, S., Parmentie, M., Ménez, B., Guyot, F., 2009. Experimental and numerical modelling of bacterially induced pH increase and calcite precipitationn in saline aquifers. Chem. Geol. 265, 44–53.
Eanes, E.D., Gillessen, I.H., Posner, A.S., 1965. Intermediate states in the precipitation of hydroxyapatite. Nature 208, 365–367.
Elliott, J.C., 1994. Structure and Chemistry of the Apatites and Other Calcium orthophosphates: Studies in Inorganic Chemistry, 18. Elsevier, Amsterdam, London, New York, Tokyo.

Gao, R., van Halsema, F.E.D., Temminghoff, E.J.M., van Leewen, H.P., van Valenberg, H.J.F., Eisner, M.D., Giesbers, M., van Boekel, M.A.J.S., 2010. Modelling ion composition in simulated milk ultrafiltrate (SMUF) I: influence of calcium phosphate precipitation. Food Chem. 122 (3), 700–709.
Giesen, A., 1999. Crystallization process enables environmental friendly phosphate removal at low costs. Environ. Technol. 20 (7), 769–775.
Grases, F., Söhnel, O., Vilacampa, A.I., March., G., 1996. Phosphates precipitating from artificial urine and fine structure of phosphate renal calculi. Clin. Chim. Acta 244 (1), 45–67.
Hoffmann, R.J., 1977. Phosphorus Rremoval in the Modified Activated Sludge Process. Research Report W22, Department of Civil Engineering University of Cape Town, South Africa.
House, W.A., Donaldson, L., 1986. Adsorption and coprecipitation of phosphate on calcite. J. Colloid Interface Sci. 112 (2), 309–324.
Jardin, H., Pöpel, J., 1996. Influence of the enhanced biological phosphorus removal on the waste activated sludge production. Water Sci. Technol. 34 (1–2), 17.
Johnsson, M.S.A., Nancollas, G.H., 1992. The role of brushite and octacalcium phosphate in apatite formation. Crit. Rev. Oral Biol. Med. 3 (1-2), 61–82.
Koutsoukos, P., Amjad, Z., Tomson, M.B., Nancollas, G.H., 1980. Crystallization of calcium phosphates: a constant composition study. J. Am. Chem. Soc. 27, 1553–1557.
Lazic, S., 1995. Microcrystalline hydroxyapatite formation from alkaline solutions. J. Cryst. Growth 147 (1–2), 147–154.
Lemaire, R., 2007. Development and Fundamental Investigations of Innovative Technologies for Biological Nutrient Removal from Abattoir Wastewater. Ph.D. Thesis. University of Queensland, Australia.
Liu, Y., Tay, J.-H., 2004. State of the art of biogranulation technology for wastewater treatment. Biotechnol. Adv. 22 (7), 533–563.
Loewenthal, R.E., Ekama, G.A., Marais, G.R., 1989. Mixed weak acid/base systems part I—mixture characterization. Water SA 15, 1.
Lundager-Madsen, H.E., Christensson, F., 1991. Precipitation of calcium phosphate at 40 °C from neutral solution. J. Cryst. Growth 114 (4), 613–618.
Lundager-Madsen, H.E., Christensson, F., Chernoc, A.A., Polyak, L.E., Suvrova, E.I., 1995. Crystallization of calcium phosphate in microgravity. Adv. Space Res. 16 (8), 65–68.
Mañas, A., Spérandio, M., Biscans, B., 2011. Biologically induced phosphorus precipitation in aerobic granular sludge process. Water Res. 45, 3776–3786.
Maurer, M., Boller, M., 1999. Modelling of phosphorus precipitation in wastewater treatment plants with enhanced biological phosphorus removal. Water Sci. Technol. 39 (1), 147–163.
Maurer, M., Abramovich, D., Siegrist, H., Gujer, W., 1999. Kinetics of biologically induced phosphorus precipitation in waste-water treatment. Water Res. 33 (2), 484–493.
Meyer, J.L., Weatherall, C.C., 1982. Amorphous to crystalline calcium phosphate phase transformation at elevated pH. J. Colloid Interface Sci. 89 (1), 257–267.
Monstastruc, L., 2003. Modélisation et optimisation d'un réacteur en lit fluidisé de déphosphatation d'effluents aqueux. Ph.D. Thesis. INPT and UPS Toulouse III.
Morgenroth, E., Sherden, T., Van Loosdrecht, M.C.M., Heijnen, J.J., Wilderer, P.A., 1997. Aerobic granular sludge in a sequencing batch reactor. Water Res. 31 (12), 3191–3194.
Murray, K., May, P.M., 1996. Joint Expert Speciation System (JESS). An International Computer System for Determining Chemical Speciation in Aqueous and Non-Aqueous Environments. Supplied by Murdoch University, Murdoch 6150, Western Australia and the Division of Water Technology, CSIR, P.O. Box 395, Pretoria, South Africa.
Musvoto, E.V., Wentzel, M.C., Loewenthal, R.E., Ekama, G.A., 2000a. Integrated chemical-physical processes modeling-I. Development of a kinetic-based model for mixed weak acid/base systems. Water Res. 34 (6), 1857–1867.
Musvoto, E.V., Wentzel, M.C., Ekama, G.A., 2000b. Integrated chemical–physical processes modeling-II. Simulating aeration treatment of anaerobic digester supernatants. Water Res. 34 (6), 1868–1880.
Nancollas, G.H., Koutsoukos, P.T., 1980. Calcium phosphate nucleation and growth in solution. Prog. Cryst. Growth Charact. 3 (1), 77–102.
Nancollas, H.G., Wu, W., 2000. Biomineralization mechanisms: a kinetics and interfacial energy approach. J. Cryst. Growth 211, 137–142.
NIST database. Searchable Bibliography of Fundamental Constants. 〈http://www.nist.gov/pml/data/physicalconst.cfm〉 (consulted on January 2011).
Paraskeva, C.A., Charalambous, P.C., Stokka, L.E., Klepetsanis, P.G., Koutsoukos, P.G., Read, P., Ostvold, T., Payatakes, A.C., 2000. Sandbed consolidation with mineral precipitation. J. Colloid Interface Sci. 232, 326–339.
Parkhurst, D.L., 2000. PHREEQC 2.2—A Computer Program for Speciation, Reaction-Path, Advective transport and Inverse Geochemical Calculation. US Geological Survey, Colorado.
Posner, A.S., Betts, F., 1975. Synthetic amorphous calcium phosphate and its relation to bone mineral structure. Acc. Chem. Res. 8, 273–281.
Seckler, M.M., Bruinsma, S.L., van Rosmalen, G.M., 1996. Phosphate removal in a fluidized bed I—identification of physical processes. Water Res. 30 (7), 1585–1588.
Serralta, J., Ferrer, J., Borrás, L., Seco, A., 2004. An extension of ASM2d including pH calculation. Water Res. 38 (19), 4029–4038.
Song, Y., Hahn, H.H., Hoffmann, E., 2001. The effects of pH and Ca/P ratio on the precipitation of calcium phosphate. In: Proceedings of the Second International Conference on Recovery of Phosphate from Sewage and Animal Wastes, Holland, 12th and 13th March.
Tomazic, B., Tomson, M., Nancollas, G.H., 1975. Growth of calcium phosphates on hydroxyapatite crystals: the effect of magnesium original research article. Arch. Oral Biol. 20 (12), 803–808.
Tsuge, H., Tanaka, Y., Yoshizawa, S., Kuraishi, T., 2002. Reactive crystallization behavior of calcium phosphate with and without whey protein addition. Chem. Eng. Res. Des. 80 (1), 105–110.
United Nations of Environment Program Yearbook, 2011. Emerging Issues in our Global Environment.
Wan, J., Spérandio, M., 2009. Possible role of denitrification on aerobic granular sludge formation in sequencing batch reactor. Chemosphere 75 (2), 220–227.
Weiner, S., 2008. Biomineralization: a structural perspective. J. Struct. Boil. 163 (3), 229–234.